RSC Advances

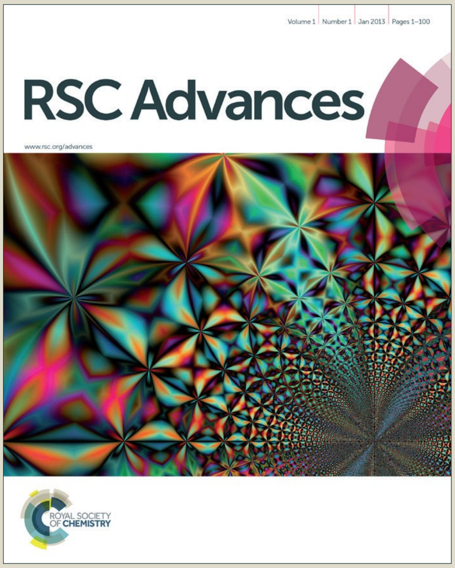

ROYAL SOCIETY OF CHEMISTRY

www.rsc.org/advances

Synthesis of Sn-Co@PMMA nanowire arrays by electrodeposition and in situ polymerization as a high performance lithium-ion battery anode

Haowen Meng [a], Hongyan Yang [a], Xiaohui Yu [a], Peng Dou [a], Daqian Ma [a] and Xinhua Xu [a,b,*]

[a] School of Materials Science and Engineering, Tianjin University, Tianjin 300072, P.R. China. E-mail:xhxu_tju@eyou.com; Tel:+86-22-2740627. Fax: +86-22-2740627

[b] Tianjin Key Laboratory of Composite and Functional Materials, Tianjin 300072, P.R. China

Abstract

Transition metals have attracted much attention for their high energy density in lithium-ion batteries (LIBs). However, the huge volume change and the fast capacity fading still limit their application. If the microstructure of the electrode materials can be designed properly, the volume change problems encountered during lithiation and delithiation could be alleviated to some extent. Here, a novel three-dimensional (3D) hybrid Sn-Co nanowire arrays coated by poly (methyl methacralate) (Sn-Co@PMMA NWs) is synthesized via a simple electrodeposition method followed by in situ emulsion polymerization. The electrode structure is well preserved after repeated Li-ion insertion/extraction, indicating that the positive synergistic effect of the Sn-Co NWs and uniform PMMA layer could effectually accommodate the volume expansion of tin anode materials. The electrochemistry results demonstrate that the Sn-Co@PMMA NWs electrode exhibits a high reversible capacity, a high initial coulombic efficiency, a good rate capability, and an improved capacity retention

compared with the bare Sn-Co NWs electrode. This proposed nanoengineering strategy is proven to be an ideal candidate for the development of high performance anode for LIBs.

1. Introduction

Lithium-ion batteries (LIBs) are currently the predominant power source for various portable electronic devices.[1, 2] They are also a potential power source for future pure electric vehicles (PEVs) and hybrid electric vehicles (HEVs).[3] At present, graphite is normally used as an anode material for LIBs, but it has a relatively low theoretical capacity (372 mA h g^{-1}). With the increasing demand of higher performance, the common commercial LIBs can not satisfy the demanding, which stimulates researchers to explore novel electrode materials to substitute the traditional materials. Tin-based intermetallic materials have attracted much interest as replacements for the conventional carbonaceous anode materials of LIBs, because the Sn in these materials has higher theoretical capacitance ($Li_{4.4}Sn$: 994 mA h g^{-1}) than that of graphite (LiC_6: 372 mA h g^{-1}). However, the key problem of a pure Sn anode is the large volume change during the alloying/dealloying process of lithiation.[4] The volume change would induce both mechanical failure and loss of electrical contact at the electrode, resulting in very rapid capacity fading. To overcome these drawbacks, there are two methods to improve the cycling performance of Sn-based anode materials. One is adopting mixed-conductor matrix to form active/inactive alloy system. The inactive metal is induced not only to enhance the mechanical strength and electron transfer dynamic but also to partly alleviate the mechanical stress caused by the volume change in the process of insertion and extraction of lithium.[5-9] Another method is using nanosized Sn based anode materials, which can also reduce volume change and restrain stress.[10-13]

Among various nanostructures, nanowire electrodes have recently attracted great interests.[14] Nanowire technology combined with such intermetallic compounds as Sn-Cu, Sn-Ni, and Sn-Co has several advantages: the inactive matrix of Cu/Ni/Co could limit volume change and prevent active materials agglomeration; the interspace among NWs could not only ease volume expansion in repetitive lithium insertion and extraction reactions, but also be in favour of electrolyte access, thus leading to high electrode/electrolyte contact area. Besides, NWs are well connected to the current collector, the need for binders or conducting additives that add additional weight is eliminated.[15-17]

However, the high aspect ratio of long nanowires may lead to agglomeration, and then result in the blocked Li-ion diffusion, reduced surface area, and the increased stress in the agglomerated nanowire arrays, which can dramatically degrade the electrochemical performance of nanowire array electrodes. In addition, the unstable solid electrolyte interphase (SEI) films formed during Li^+ insertion may decompose completely, catalyzed by transition metals formed during the Li^+ extraction processes. Requirement for repeated formation/decomposition of the SEI layer may lead to fast capacity fading.[18, 19] Typically, one strategy to stabilize the surface and structure is to create core/shell nanostructures. Conformal coating of Sn-Ni electrode materials with PEO or PMMA has shown fast rates of charge and discharge maintaining high energy densities. Such polymer coatings not only serve as the electrolyte functionality but also could help in controlling and forming stable SEI films formation on the high surface area nanostructured electrodes owning to the high strength and dimensional stability.[20, 21]

Ferrara and co-workers have prepared the Sn-Co nanowires inside the channels of anodic alumina membrane by potentiostatic deposition.[22] However, they couldn't investigate the electrochemical charge-discharge behaviors of Sn-Co NWs. Here we report the detailed electrochemical characterization of nanoarchitectured Sn-Co NWs electrode. Co is induced not only to enhance the mechanical strength and electron transfer dynamic along the 1D nanowires, but also to partly alleviate the mechanical stress caused by the volume change of the Sn phase. Meanwhile, in order to improve the stability and rate performance of the nanostructured electrode, we design a architecture composed of Sn-Co alloy nanowire arrays with an ultrathin conformal poly (methyl methacralate) (PMMA) coating. We choose the PMMA as the coating layer because it exhibits considerable wettability for organic liquid electrolyte and the shells could become a gel with some characteristics of the gel polymer electrolyte after activation by the liquid electrolyte.[20, 23] In addition, the electron donating C=O group of PMMA is highly active in forming the coordination with cations. So it could increase the ionic conductivity and decrease the interfacial impedance. Although Ajayan et al. synthesized the Sn-Ni@PMMA NWs through the drop coating technique, it is still a challenge to obtain uniform and strongly contact coatings around nanostructured electrode materials.[21] Unlike usual cases, we obtain the PMMA coating through in situ emulsion polymerization. This method could greatly enhanced interfacial compatibility between metals and polymer by treating the surface of metal hydrophobically and imparting conformational anchorage factor at metal interfaces, which could effectively restrict the expansion of anode materials.[24,25] It is shown that the Sn-Co@PMMA electrode by in situ suspension polymerization exhibits appealing advancement of Li^+ storage property, delivering high capacity, long cycle lifespan, and high rate capability than bare Sn-Co NWs electrode.

2. Results and discussion

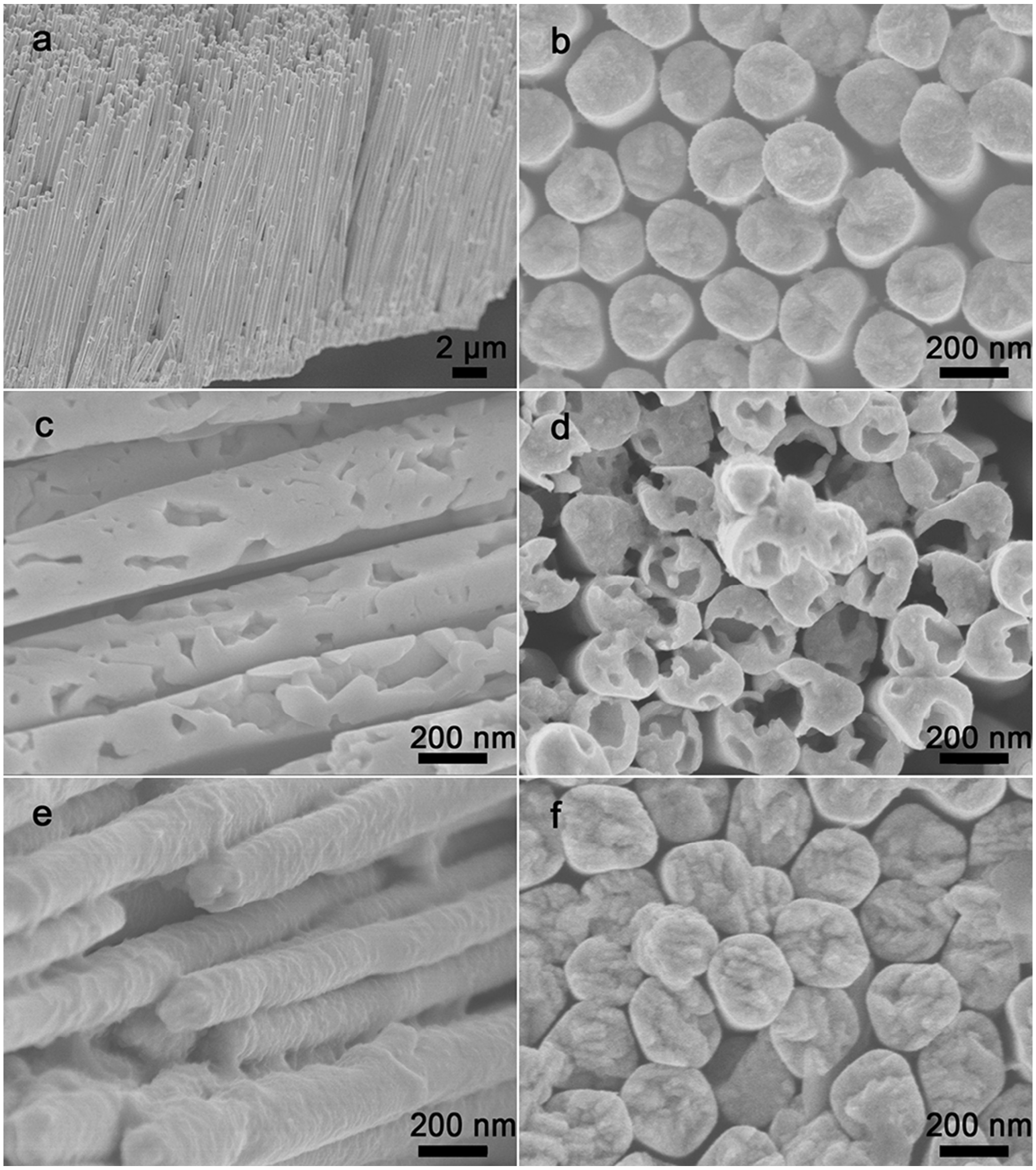

Fig. 1 SEM image of (a, b) bare Sn-Co NWs, (c, d) Sn-Co@PMMA NWs 1 and (e, f) Sn-Co@PMMA NWs 2.

The morphology of Sn-Co NWs and Sn-Co@PMMA NWs are shown in Fig. 1. The Sn-Co@PMMA NWs 1 and Sn-Co@PMMA NWs 2 are synthesized through drop coating technique and in situ suspension polymerization, respectively. It can be seen from Fig. 1a-b that the as-prepared Sn-Co NWs are smooth and perpendicular to the substrate. The diameters of the Sn-Co NWs are estimated to be about 200 nm, while the lengths are 22 μm, which is much longer than that of previously reported Sn-Co NWs (2-16 um) by Sunseri's group.[22] We emphasize here that the greater aspect ratio nanowire is meaningful for LIBs: First, a greater aspect ratio could support more active material; second, a greater aspect ratio can palliate the problems of the slow electrochemical kinetics and sluggish transport rate by increasing the contact area between the active materials and the electrolyte. Fig. 1c-d is SEM images of Sn-Co@PMMA nanowire arrays by drop coating technique. As we can see the PMMA layer is full of bumps and hollows resulting from the poor fluidity of polymer solution on the surface of alloy and that will cause a weight imbalance during lithiation and delithiation, leading to the poor structural stability. The Sn-Co@PMMA nanowire arrays through in situ emulsion polymerization are shown in Fig. 1e-f, from which we can notice that the surface of nanowires is a slightly rough and the diameter becomes larger than the bare NWs. Besides, the space between nanowires in Fig. 1f is smaller than that of Fig. 1b, indicating the successful deposition of PMMA layer. Though more severe agglomeration is unavoidable with longer nanowire arrays and smaller space, the polymer electrolyte PMMA coating layer can serve as a geometrical separator to avoid the agglomeration effectively.[21] So this construction that combines the 3D nanowires structure and flexible confining coating is expected to contribute to an upgraded cycling performance of anode materials.

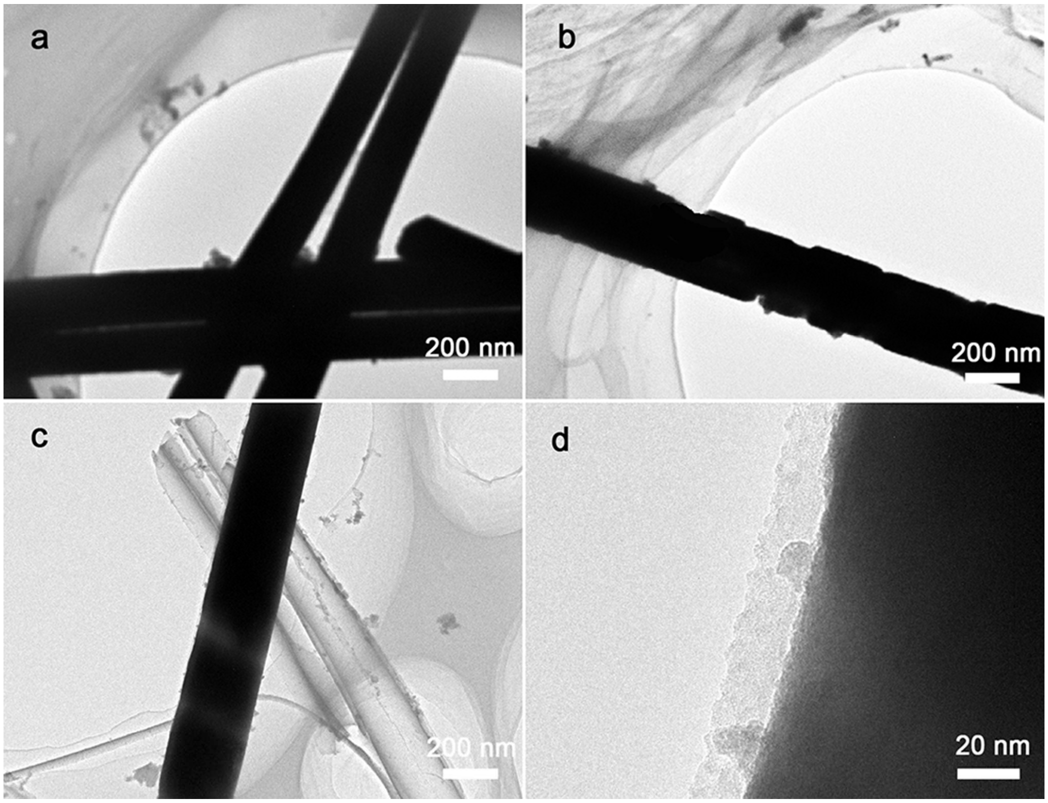

Fig. 2 TEM image of (a) Sn-Co NWs and (b) Sn-Co@PMMA NWs 1; (c) TEM and (d) HR-TEM images of Sn-Co@PMMA NWs 2.

The conformal nature of the PMMA coating around the nanowires is observed for all the Sn-Co NWs imaged using TEM. Compared with the bare NWs (Fig. 2a), both Sn-Co@PMMA NWs 1 (Fig. 2b) with a slight irregularity in the surface and Sn-Co@PMMA NWs 2 have the larger diameter, also suggesting the successful deposition of PMMA layer. As depicted in Fig. 2d, the thin electrolyte (PMMA) layer is about 15 nm. The SEM and TEM images clearly demonstrate that the Sn-Co@PMMA NWs produced by in situ emulsion polymerization are much better than that through drop coating technique.

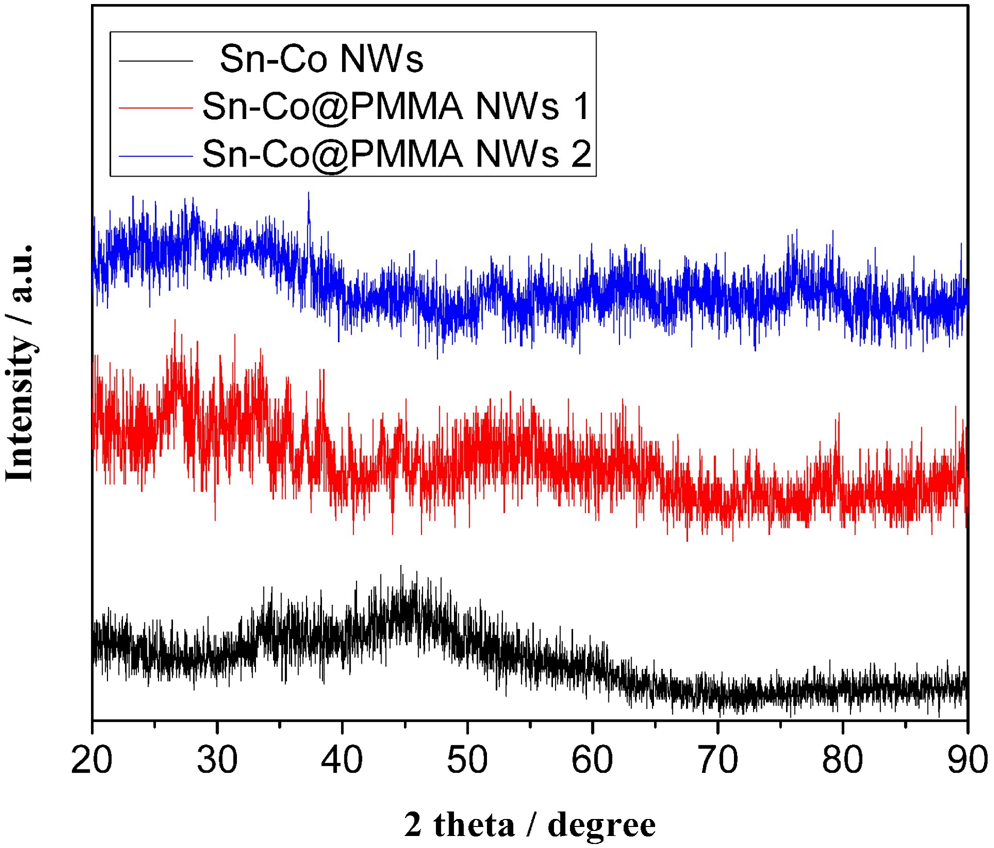

Fig. 3 XRD patterns of Sn-Co NWs, Sn-Co@PMMA NWs 1 and Sn-Co@PMMA NWs 2.

The crystallographic structure of Sn-Co NWs and Sn-Co@PMMA NWs is further analyzed by XRD as shown in Fig. 3. The XRD patterns do not show any peak having significant intensity for the three samples. On this basis, we can conclude that the deposits are essentially amorphous. Moreover, energy-dispersive X-ray spectroscopy (EDS) (Fig. S1) was carried out to investigate the elemental composition of the deposit, which verified the existence of Sn and Co with a ratio of 71.03: 28.97, 70.13: 29.87 and 68.97: 31.03 (by atomic %) for Sn-Co NWs, Sn-Co@PMMA NWs 1 and Sn-Co@PMMA NWs 2, respectively. So it was considered that the $Sn_{70}Co_{30}$ would be referred to as a metastable phase. Abundant research confirmed that

$Sn_{1-x}Co_x$ alloy for $0.28 < x < 0.43$ possessed the most stable electrochemical performance.[26,27] Therefore, good Li^+ storage capability was expected in our $Sn_{70}Co_{30}$ composites.

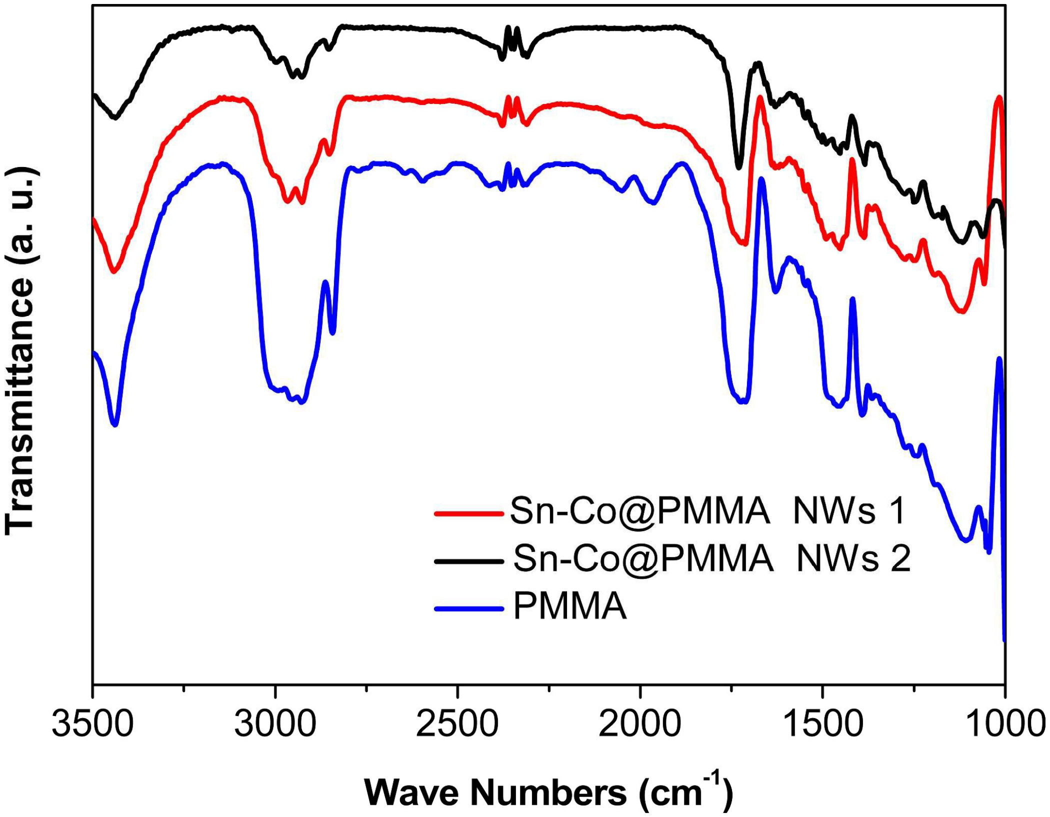

Fig. 4 FT-IR spectra of PMMA, Sn-Co@PMMA NWs 1 and Sn-Co@PMMA NWs 2.

The abovementioned result is also supported by the FT-IR spectra shown in Fig. 4. Fig. 4 shows the characteristic absorption of PMMA in the samples, where indicates that the main polymer chains of the Sn-Co@PMMA composites are similar to that of the PMMA. It can be seen that the characteristic absorption bands are clearly visible in the region of 2972, 2929, 2853, and 1376 cm^{-1} for stretching vibration of C-H in methylene and methyl groups.[28] Besides, a stronger band at 1722 cm^{-1} and a relatively strong band at 1241 and 1149 cm^{-1} due to the C=O and C–O stretches can be observed.[29] These peaks indicate that the Sn-Co core NWs have been well doped in the PMMA shells. To investigate the weight loss of the hollow Sn-Co@PMMA composites, thermogravimetric analysis was carried out in air. As shown in Fig. S2, the TG curves show weight loss of 5.4% for Sn-Co@PMMA NWs 1 and 6.2% for Sn-Co@PMMA NWs 2 from 230℃ to 400℃, which indicates the decomposition of PMMA in air.

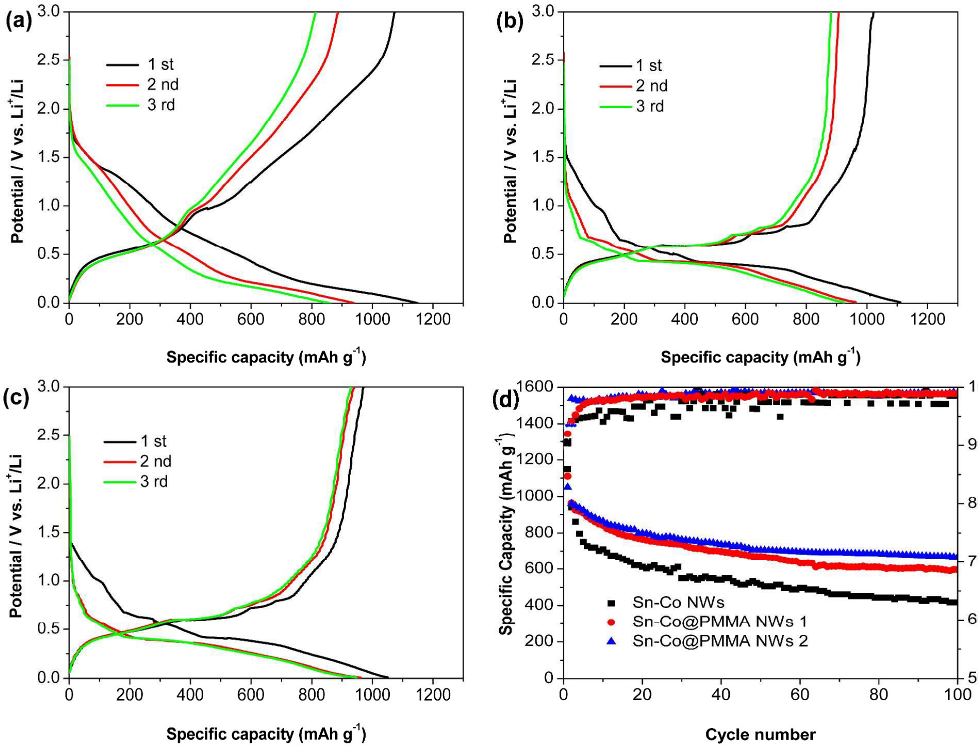

Fig. 5 Discharge-charge curves of (a) Sn-Co NWs electrode, (b) Sn-Co@PMMA NWs 1 electrode and (c) Sn-Co@PMMA NWs 2 electrode; (d) Cycling performance and coulomb efficiency of Sn-Co NWs electrode, Sn-Co@PMMA NWs 1 electrode and Sn-Co@PMMA NWs 2 electrode.

Motivated by the unique structure of the core-shell nanostructure array electrodes, we performed the lithium storage test as anodes. From the CV curves of Fig. S3, there is a large cathodic slope arises from~1.5 V in the first discharge process of Sn-Co

NWs electrode, which should be closely ascribed to the electrolyte decomposition and the formation of SEI layer. And this cathodic slope will result in large irreversible capacity loss. However, the initial irreversible reduction peak of Sn-Co@PMMA NWs electrodes is much smaller than bare Sn-Co NWs electrode, suggesting the lower initial irreversible capacity. The reduction peak at 0.24 V is due to the electrochemical reaction of Sn component in the Sn-Co composite involving the formation of Li_xSn alloy.[30, 31] Upon charge, two current peaks appear at around 0.5 and 0.68 V, which is ascribed to the delithiation process of Li_xSn. Fig. 5a-c displays the charge-discharge voltage profiles of representative cycles of Sn-Co NWs and Sn-Co@PMMA NWs electrode tested by galvanostatic cycles between 0.01 and 3.00 V vs. Li at 0.1 C. As we can see, a large slope between 1.5 and 0.6 V is also noticed in the first discharge process for the bare Sn-Co NWs electrode, which is in consistent with the CV curves. The plateau at 0.6 V and the subsequent sloping region gradually falling to 0.01 V correspond to the lithiation process of various stages of the Sn-Co alloy, as described by the following equation

$$Co_ySn + xLi^+ + xe^- \rightarrow Li_xSn + yCo \qquad (0 < x < 4.4) \qquad (1)$$

When lithium reacts with Sn, the inactive Co would be displaced or extruded from the parent phase. The extruded component Co is dispersed into the host lattice and can act as buffer particles which limit the volume expansion. However, the change trend of initial three discharge-charge curves of the Sn-Co@PMMA NWs are different from the Sn-Co NWs anode， indicating that PMMA has some influence on the charge/discharge reaction process of electrode materials. Specifically, for the second and third cycles, the discharge profiles (corresponding to the lithiation process) of Sn-Co@PMMA NWs electrode overlap to a great extent, especially the Sn-Co@PMMA NWs 2, which suggests the Sn-Co@PMMA NWs electrode by in situ emulsion polymerization possesses more steady Li^+ storage properties than Sn-Co NWs and Sn-Co@PMMA NWs 1 electrode. This may attribute to the high ion-conductive and uniform coating of PMMA. Sn-Co NWs and Sn-Co@PMMA NWs 1, 2 electrode show an initial discharge capacity of 1177 mA h g^{-1}, 1110 mA h g^{-1} and 1045 mA h g^{-1} with a high first charge capacity nearly 1042 mA h g^{-1}, 1021 mA h g^{-1} and 977 mA h g^{-1}, giving a high coulomb efficiency of 88.5%, 92.0% and 93.5%, respectively. As far as we know, the coulombic efficiency for the first cycle in this study is much higher than that for most tin-based anode materials previously reported.[32-34] Such a high coulombic efficiency is not only owing to the cushioning effect of Co, but also the prompt electrochemical reactions (due to the larger specific surface area) and fast charge transferring (duo to the shorter ion transport distance). Moreover, the coulombic efficiency of the Sn-Co@PMMA NWs 2 electrode at the second cycle increases to 98.1%, while the coulombic efficiency of Sn-Co NWs and Sn-Co@PMMA NWs 1 electrode is still about 94.2%. This phenomenon could be explained by the different changing process of array and solid electrolyte interphase on the electrode surface. During the first cycle, they all facilitate the decomposition of electrolyte to form SEI layer on the electrode surface and show a higher capacity than the theoretical capacity. But during the following cycles, the repetitive volume change not only leads to the Sn-Co alloy pulverization and isolation but also makes it difficult to form a stable protection layer to maintain the SEI layer, which result in the degradation of electrolyte and the cell to fail.[35, 36] While uniform PMMA layer could ease the volume expansion and keep the mechanical integrity, so the SEI layer formed outside the NWs is not ruptured during cycling.[37] Just as shown in Fig. 5d, after the coulombic efficiency of Sn-Co@PMMA NWs 2 reaches 98.1% at the second cycle, the others most keep steady at more than 99% thereafter, higher than that of the bare nanowire array. This clearly demonstrates the stable electrode structure of Sn-Co@PMMA and the effectively avoided harmful reactions between electrolyte and Sn-Co alloy through the conformal coating of PMMA. The cycle performance of the Sn-Co@PMMA NWs and Sn-Co NWs is evaluated shown in Fig. 5d. It is observed that the Sn-Co@PMMA NWs 2 electrode demonstrates an excellent cycling stability with a high reversible capacity of 668 mA h g^{-1} after 100 cycles, which corresponds to 63.9% capacity retention against at the 1st discharge capacity. This is more promising than that of fussy Sn-Co nanoarchitectured electrode conducted by Du, which shows 55.6% capacity retention against at the 1st discharge capacity after 90 cycles, certifying that the conformal coating would contribute to better electrochemical property than bare electrode materials.[38] In our research, the capacity of Sn-Co NWs fades rapidly to a value lower than 417 mA h g^{-1} after 100 cycles, only 35.4% capacity retention against at that of the 1st discharge capacity. The cycle performance of the Sn-Co@PMMA NWs is markedly much better than the bare Sn-Co NWs electrode. The improved cyclability of Sn-Co@PMMA NWs 2 electrode can be ascribed to the unique multifunctional composite structure of the thin polymer PMMA coating layer as a buffer to hold stresses caused by volume change. The relationship between morphology of PMMA and cycling properties was investigated by charge/discharge Sn-Co@PMMA NWs 1 in half-cell. The capacity fades fast in the first 60 cycles, indicating the electrochemical performance declines as the PMMA layer is nonuniform. However, because the PMMA coating NWs electrode could meaningfully improve the cyclabilty than the bare NWs electrode, the property of coating layer should be devoted further effort to make it suitable for abundant active materials.

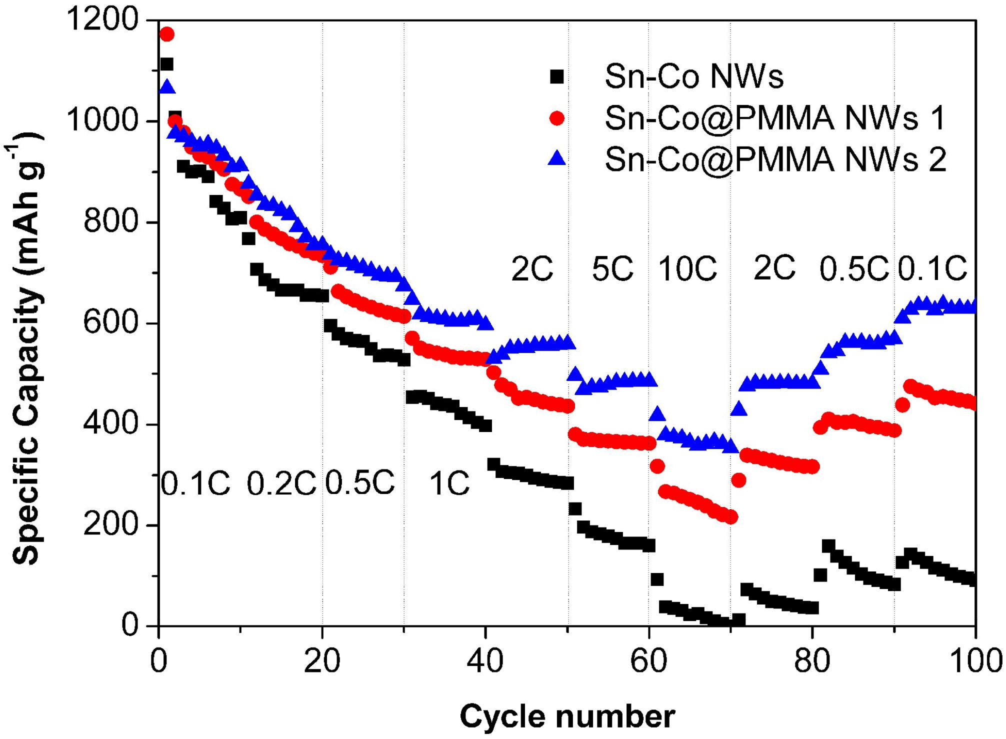

Fig. 6 Rate capabilities of Sn-Co NWs electrode, Sn-Co@PMMA NWs 1 electrode and Sn-Co@PMMA NWs 2 electrode.

In order to confirm the feasibility of uniform PMMA coating electrode for LIBs application, cycle rate capability tests were conducted at various current rates ranging from 0.1 C to 10 C(Fig. 6). The PMMA coating electrode by in situ emulsion polymerization delivers reversible capacities of 902, 755, 674, 597, 559 and 485 mA h g^{-1} at the increasing current rates of 0.1, 0.2, 0.5, 1, 2, and 5 C every 10 cycles, respectively. Even at a high current rate of 10C, the specific capacity still retains a value of approximately 353 mA h g^{-1}. Moreover, when the current rate decreases back to 0.1 C, specific area capacity of around 633 mA h g^{-1} can be restored after 100 cycles, indicating the excellent tolerance against the high current density of Sn-Co@PMMA anode materials. Under the same conditions, the Sn-Co@PMMA NWs 1 demonstrated noticeable decay after 30 cycles, but the capacity decrease with the following cycles was less pronounced at high current densities > 2 C. For comparison, the capacities of the Sn-Co NWs array electrode decay even more significantly, with a capacity of about almost 0 mA h g^{-1} at a current rate of 10 C after 70 cycles. The performance of bare Sn-Co NWs also has a large hysteresis due to the current densitiese-resetting the current density back to 2 C, after high current density, not only do not recover to the original capacity but the value is rapidly declining.

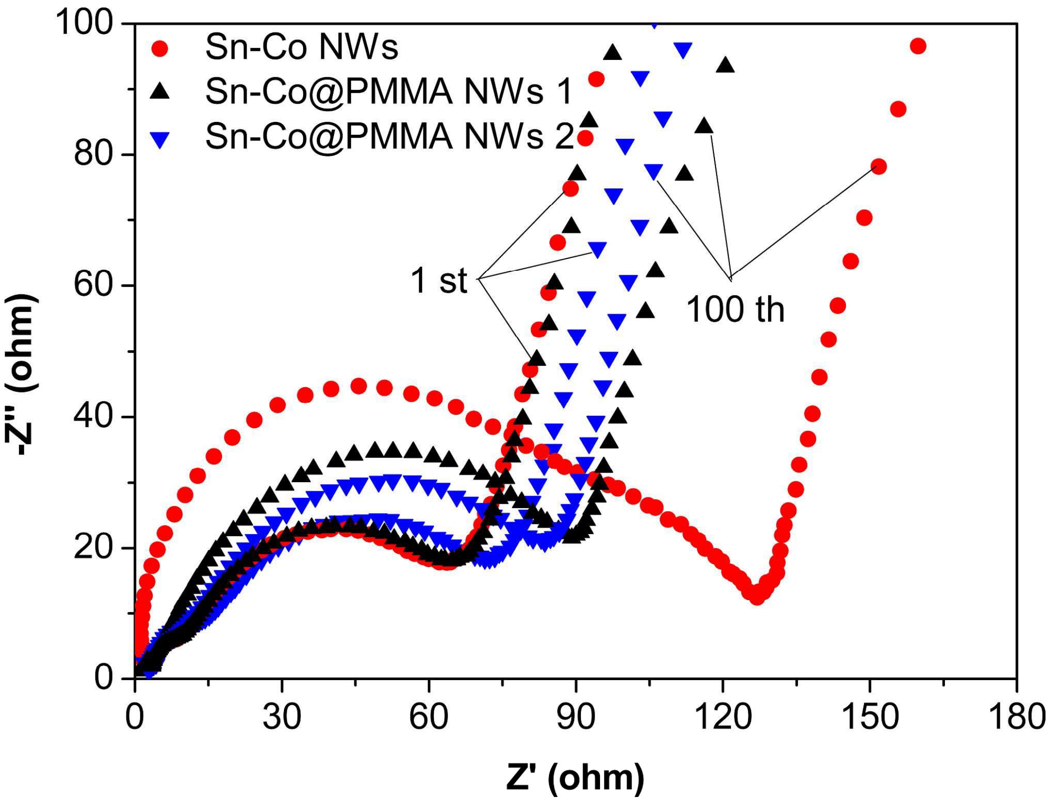

Fig. 7 The EIS spectra of Sn-Co NWs electrode, Sn-Co@PMMA NWs 1 electrode and Sn-Co@PMMA NWs 2 electrode after the first and 100 cycles, respectively.

Actually, the cycle stability and high rate capability are mostly related to the thickness of SEI film, lithium-ion diffusion, and interfacial charge transfer process in a composite. In order to understand the superior electrochemical performance, electrochemical impedance spectroscopy (EIS) measurements of the Sn-Co@PMMA NWs 1, 2 and Sn-Co NWs electrode were conducted after the 1st and 100th cycles at a current density of 0.1 C (Fig. 7). The impedance curve of each sample is consisted of a semicircle in the medium frequency region and a straight line in the low-frequency region. The intercept at the real impedance axis in the high frequency region is normally regarded as electrical conductivity of the electrolyte, separator, and electrodes, and it remains about the same after 100 cycles for the two electrodes. The diameter of the semicircle in the high frequency range reflects the resistance of SEI layer formed on the surface of electrode (R_{sf}) and the charge-transfer resistance (R_{ct}) which is related to the electrochemical reaction between the electrode and the electrolyte. After 1st cycle, the $R_{(sf+ct)}$ impedance of Sn-Co@PMMA NWs is similar with that of Sn-Co NWs, indicating that they have the semblable SEI layer and charge-transfer resistance. After 100th cycles, the $R_{(sf+ct)}$ impedance of the Sn-Co@PMMA NWs 2 is much smaller than that of the Sn-Co NWs, suggesting the stable thin SEI layer and quick lithium-ion diffusion rate. This result confirms that the incorporation of PMMA coating through in situ emulsion polymerization is an effective way for enhancing the stability of electrode structure and the ion transport, which leads to a significant improvement in the electrochemical performance.

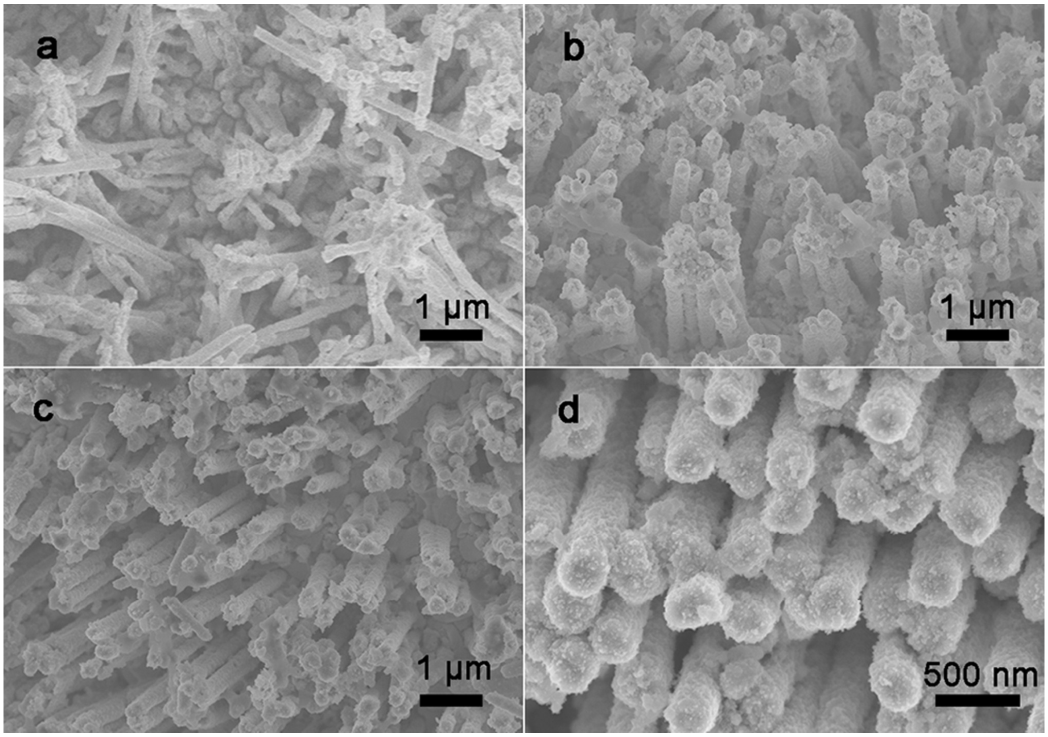

Fig. 8 SEM images of Sn-Co NWs electrode, Sn-Co@PMMA NWs 1 electrode and Sn-Co@PMMA NWs 2 electrode after 100 cycles.

To confirm that the uniform PMMA coating electrode was more capable of maintaining the structure integrity than the bare one, we acquired the SEM images of the electrodes after cycling and displayed them in Fig. 8a, b, c-d for samples Sn-Co NWs and Sn-Co@PMMA NWs 1, 2, respectively. As we can see, after 100 charge/discharge cycles, a large number of nanowires break off from the root and no longer show a clear structure for the sample of Sn-Co NWs. The Sn-Co NWs alloy inflated and bended because of the lithium insertion and volume expansion; during lithium extraction and volume recovery, they contracted and self-adjusted into microflakes to alleviate the strains inside the nanowire, resulting in the arrays falling down. As we know, once the active materials break away from the substrate, the Li^+-ion transport through the electrolyte as well as the electronic conduction is decreased, which reduces the coulombic efficiencies and cycle life significantly. On the contrary, Sn-Co@PMMA NWs electrodes basically maintain their original array architecture after 100 cycles. No exfoliation and collapse phenomenon can be evidenced. Especially the Sn-Co@PMMA NWs 2, no agglomerates can be observed and we can see each NWs clearly. As shown in figure 7d, after 100 cycles, the diameter and morphology of nanowires has no apparent change. And there still exist enough spaces between adjacent nanowires and that could largely absorb the volume expansion. Despite the fact that the smooth wall surface becomes rough due to the repeated lithiation/delithiation reactions, the integral structure remains almost the same with the pristine product. Further more, the TEM images (Fig. S4) also prove that the Sn-Co@PMMA NWs could maintain their pristine morphology and the SEI film formed around PMMA layer is not ruptured after cycling, which is consistent with our previous research.[39] However, the bare Sn-Co NWs suffer a repeated breaking and formation of thick SEI layer during cycling leading to loss of cyclic lithium, consumption of electrolyte, and compromised electrical contact between active materials, and hence, continuous capacity fading. These results clearly demonstrate that the uniform coating layer of PMMA can effectively suppress the electrode from inflation and pulverization and consequently result in the formation of a stable and thin SEI layer on the surface of the cycled electrode.

Overall, several factors might have contributed to the excellent electrochemical performance of the Sn-Co@PMMA NWs 2 composite anodes. Firstly, three-dimensional nanowires electrode possesses the fast Li^+ transport dynamic and high utilization of electrode materials on account of short ion diffusion lengths and large active materials' exposure; Secondly, the introduction of Co and the electrically connected to the Cu current collector could improve the electronic conductivity without adding any polymer binder and carbon black. Thirdly, the residual void volume after the PMMA coating between each nanowires not only allows easy penetration of the electrolyte resulting in a short Li-ion pathway, but also helps to accommodate the large volume change during Li^+ insertion/extraction resulting in better cycle capability. Last but not least, the ultrathin PMMA coating can help to avoid the direct contact interface area between Sn-Co alloy and electrolyte, which effectively reduces the degree of the repeated formation/decomposition of SEI film. Besides, the PMMA layer can also provides elastic accommodation to restrain substantial electrode agglomeration and pulverization, thus maintaining good cycle stability.

3. Conclusions

In summary, the Sn-Co@PMMA composite anodes have been constructed using a facile electrodeposition and in situ emulsion polymerization. It is demonstrated that the Sn-Co@PMMA NWs electrode exhibits excellent electrochemical performance in terms of reversible specific capacity and cycling stability, especially where a capacity of about 668 mA h g^{-1} after 100 cycles has been realized. The enhanced cycling performance is attributed to the well designed alloy nanowire array with uniform PMMA coating, which can not only buffer the volume change, but also improve the ionic conductivity and maintain excellent structural/interfacial stability during cycles. Above all, this novel structure can be further extended for other anode materials, and it is of great potential for next generation energy storage and other applications.

ASSOCIATED CONTENT

Supporting Information. Details about experimental methods, TG curves, cyclic voltammetric curves and EDS microanalysis of the synthesized samples.

Acknowledgements

This work was financially supported by the National Natural Science Foundation of China (No.51143009 and 51273145).

References

1 Y. Zhong, X.F. Li, Y. Zhang, R.Y. Li, M. Cai and X.L. Sun, Appl. Surf. Sci. 2015, 332, 192.

2 P.G Bruce, Solid State Ionics 2008, 179, 752.

3 S. Kundu, S. Sain, M. Yoshio, T. Kar, N. Gunawardhana and S.K. Pradhan, Appl. Surf. Sci. 2015, 329, 206.

4 J.O. Besenhard, J. Yang and M. Winter, J. Power Sources 1997, 68, 87.

5 Y. Gu, F.D. Wu and Y. Wang, Adv. Funct. Mater. 2013, 23, 893.

6 W.J. Cui, F. Li, H.J. Liu, C.X. Wang and Y.Y. Xia, J. Mater. Chem. 2009, 19, 7202.

7 R. Hu, H. Liu, M.Q. Zeng, H. Wang and M. Zhu, J. Mater. Chem. 2011, 21, 4629.

8 Z. Edfouf, C. Fariaut-Georges, F. Cuevas, M. Latroche, T. Hézèque, G. Caillon, C. Jordy, M.T. Sougrati and J.C. Jumas, Electrochim. Acta 2013, 89, 365.

9 X. Fan, P. Dou, A. Jiang, D. Ma and X. Xu, ACS Appl. Mater. Interfaces 2014, 6, 22282.

10 D. Applestone and A. Manthiram, RSC Adv. 2012, 2, 5411.

11 X.F. Li, Y. Zhong, M. Cai, M.P. Balogh, D.N. Wang, Y. Zhang, R.Y. Li and X.L. Sun, Electrochim. Acta 2013, 89, 387.

12 D. H. Lee, H. W. Shim, J. C. Kim and D. W. Kim, RSC Adv. 2014, 4, 44563.

13 Y. Wang, M.H. Wu, Z. Jiao and J.Y. Lee, Chem. Mater. 2009, 21, 3210.

14 Y.G. Li, B. Tan and Y.Y. Wu, Nano Lett. 2008, 8, 265.

15 Z. Wang, N. Du, H. Zhang, J. Yu and D. Yang, J. Phys. Chem. C. 2011, 115, 23620.

16 J.Z. Chen, L. Yang, S.H. Fang, S.I. Hirano and K. Tachibana, J. Power Sources 2012, 199, 341.

17 M. Tian, W. Wang, S.H. Lee, Y.C. Lee and R.G. Yang, J. Power Sources 2011, 196, 10207.

18 G. Liu, S.D. Xun, N. Vukmirovic, X.Y. Song, P. Olalde-Velasco, H.H. Zheng, V.S.

Battaglia, L.W. Wang and W.L. Yang, Adv. Mater. 2011, 23, 4679.

19 M.Y. Nie, D.P. Abraham, Y.G. Chen, A. Bose and B.L. Lucht, J. Phys. Chem. C. 2013, 117, 13403.

20 S.R. Gowda, A. Leela Mohana Reddy, X.B. Zhan and P.M. Ajayan, Nano Lett. 2011, 11, 3329.

21 S.R. Gowda, A.L.M. Reddy, M.M. Shaijumon, X.B. Zhan, L.J. Ci and P.M. Ajayan, Nano Lett. 2010, 11, 101.

22 G. Ferrara, R. Inguanta, S. Piazza and C. Sunseri, Electrochem. Solid-State Lett. 2009, 12, K17.

23 P. Yang, P. Zhang, C. Shi, L. Chen, J. Dai and J. Zhao, J. Membr. Sci. 2015, 474, 148.

24 J.W. Shim, J.W. Kim, S.H. Han, I.S. Chang, H.K. Kim, H.H. Kang, O.S. Lee and K.D. Suh, Colloid. Surf. 2002, 207, 105.

25 G. Chen, R. Rodriguez, L. Fei, Y. Xu, S.G. Deng, S. Smirnov and H.M. Luo, J. Power Sources 2014, 259, 227.

26 J.R. Dahn, R.E. Mar and A. Abouzeid, J. Electrochem. Soc. 2006, 153, A361.

27 A.D.W. Todd, R.E. Mar and J.R. Dahn, J. Electrochem. Soc. 2006, 153, A1998.

28 T. Kuila, S. Bose, P. Khanra, N.H. Kim, K.Y. Rhee and J.H. Lee, Composites Part A 2011, 42, 1856.

29 Y.Y. Dong, Z. Gui, S.H. Jiang, Y. Hu and K.Q. Zhou, Ind. Eng. Chem. Res. 2011, 50, 10903.

30 J. Zhang and Y. Xia, J. Electrochem. Soc. 2006, 153, A1466.

31 A. Jiang, X. Fan, J. Zhu, D. Ma and X. Xu, Ionics. 2015, 21, 2137.

32 R.Z. Hu, H. Liu, M.Q. Zeng, H. Wang and M. Zhu, J. Mater. Chem. 2011, 21,

4629.

33 G. Ferrara, C. Arbizzani, L. Damen, M. Guidotti, M. Lazzari, F.G. Vergottini, R. Inguanta, S. Piazza, C. Sunseri and M. Mastragostino, J. Power Sources 2012, 211, 103.

34 X.Y. Fan, F.S. Ke, G.Z. Wei, L. Huang and S.G. Sun, Electrochem. Solid-State Lett. 2008, 11, A195.

35 C.K. Chan, R. Ruffo, S.S. Hong and Y. Cui, J. Power Sources 2009, 189, 1132.

36 P. Verma, P. Maire and P. Novák, Electrochim. Acta 2010, 55, 6332.

37 F. Han, D. Li, W.C. Li, C. Lei, Q. Sun and A.H. Lu, Adv. Funct. Mater. 2013, 23, 1692.

38 Z.j. Du and S.C. Zhang, J. Phys. Chem. C. 2011, 115, 23603.

39 X. Yu, A. Jiang, H. Yang, H. Meng, P. Dou, D. Ma and X. Xu, Appl. Surf. Sci. 2015, 347, 624.